Emergent Elastic Surfaces from Two-Dimensional Dirac Materials

Pablo A. Morales[1, 2, *] and Pavel Castro-Villarreal[3, †]

[1] *Research Division, Araya Inc., Tokyo 107-6019, Japan*
[2] *Centre for Complexity Science, Imperial College London, London SW7 2AZ, UK*
[3] *Facultad de Ciencias en Física y Matemáticas, Universidad Autónoma de Chiapas, Carretera Emiliano Zapata, Km. 8, Rancho San Francisco, C. P. 29050, Tuxtla Gutiérrez, Chiapas, México*

Temperature constraints are highly desirable in the experimental setup when seeking the synthesis of new carbon structures. Fluctuations of the Dirac field result in temperature-dependent corrections to the Helfrich-Canham formulation, which governs the classical elasticity of the membrane in equilibrium state. Here, we examine the emergent shapes allowed by the effective model up to quadratic order in Ricci curvature and discuss the constraints required to observe them. We determine the mechanical stability conditions and provide a phase diagram characterized by the appearance of a critical temperature T_c that distinguishes between carbon nanotube and fullerene phases. The observation of minimal and developable surfaces is anticipated, respectively, at the high- and low-temperature regimes.

Introduction. The rapid improvement in graphene synthesis techniques has increased interest into the problem of how morphology relates to its properties [1, 2]. Graphene can be bent to form corrugated graphene, folded to form fullerenes, rolled into carbon nanotubes, and stacked in the shape of graphite, making it the mother of graphitic materials [3]. The production of flat graphene sheet is also subject to deformations; dislocations introduce strain fields that lead to instabilities [4], these stresses are then relieved by out-of-plane ripples which manifest in the presence of the experimentally observed nanobubbles [5]. Furthermore, the Dirac-like spectrum of the low energy excitations suggests the possibility of table-top experiments as a testbed for relativistic quantum phenomena and vise-versa. In this way, the coupling of massless Dirac fermions to the sample geometry enables us to directly probe morphological effects. Indeed, the emergence of pseudo-gauge fields from the ripples in graphene modulated by curvature [6, 7] and observed in the order of 300 T [5] critically affecting the sample's electrical properties.

However, without an accurate tight-binding (TB) description for curved graphene, it becomes difficult to determine the precise field theory for low energies that allows us to model its properties. TB models for deformed graphene are usually based on position-dependent hopping integrals and a slightly deformed honeycomb lattice [4]. Curved graphene, however, generally ceases to be a crystal due to the changes in its structural lattice produced by the bending or stretching of graphene. Hence, it is not obvious how to formulate a TB model that accounts for the topological defects that make up curvature. Consistently taking into account lattice gauge symmetry of standard TB models leads to nonlinear modifications to the Dirac dynamics in curved space-time [8], see [9, 10] for other views. Resolving the breaking of translational symmetry in crystalline structures precedes a proper, effective field theoretic formulation. On the other, the perhaps more phenomenological approach of the curved-space Dirac field theory is currently considered the simplest model for investigating the electronic degrees of freedom in graphene membranes with corrugations. In fact, up to fitting via Density Functional Theory (DFT), the low energy spectrum obtained from a TB model for Gaussian bump graphene in a transverse magnetic field agrees well with the spectrum obtained using the curved Dirac model with the same conditions [11].

Grounding to an experimental set-up demands knowledge of the surface embedding and the response from the electronic degrees of freedom confined to the *membrane* at a given temperature. Actually, the self-assembly formation of carbon surfaces like carbon nanotubes, fullerenes, and carbon nanocones, among other curved graphene surfaces, is a complex phenomenon. The known experimental methods to produce these structures, like arc discharge, thermal pyrolysis, and chemical vapor deposition, among others, revealed an out-of-equilibrium process for their formation [12, 13], which is out of the known theoretical approach. However, after the complex path to achieve a piece of the curved graphene surface at an equilibrium temperature, the surface must be mechanically stabilized, considering the Dirac fermionic degrees of freedom. In fact, it has been shown that the relativistic Dirac degrees of freedom result in the tendency of the membrane to crumple [14], which seems to be consistent with the experimental observation for the transformation from graphene to fullerene [13]. The classical membrane free energy is thus corrected by a significant quantum contribution that critically affects its stability. Connection to curved graphene would also require inclusion of a non-abelian gauge field to account for topological defects [15], however, as a naïve model, one may ask *what are the experimental conditions at which a given structure may be expected?*. Basic notions of geometry and topology have led to the prediction of positively curved carbon nano-structures with unique properties and synthesized [16]. Negative curvature carbon materials, on the other hand, although proposed for more than a decade

prior the synthesis of graphene [17] have yet to be observed in the laboratory. Despite great expectations, the unknown mechanisms for its production and experimental synthesis have made its observation, uncertain.

In this paper, we investigate the role played by Dirac field thermal fluctuations on the effective spatial geometry of a Dirac material. We provide an effective *shape equation* for extremal configurations and the general conditions that such configurations represent an equilibrium configuration. Based on a naïve model for graphene membrane, we discuss the characteristic scale of some of the carbon structures observed in the lab as well as the temperatures at which these should be observed.

2D fermionic membranes. Commonly the space-time geometry used in $2D$ materials is modeled using a $2+1$ stationary space-time pseudo-Riemannian metric given by $ds^2 = -v_F^2 dt^2 + g_{ab}dx^a dx^b$, where v_F is an effective velocity associated to the $2D$ Dirac material, *e.g.* in graphene v_F is the Fermi velocity, and the spatial component of the metric, g_{ab} represents the Riemannian metric associated with the geometry of a 2-dimensional surface Σ, where $a, b = 1, 2$ are the local indices of the surface. The material sheet is embedded in $3D$ Euclidean space and thus an extrinsic description for the sheet geometry is required. The embedding functions are introduced through the mapping $\mathbf{X} : \mathscr{D} \subset \mathbb{R}^2 \to \Sigma \subset \mathbb{R}^3$, where $\mathscr{D}$ is a certain open set. In addition, it has been suggested that the Helfrich-Canham free energy [18], used in the biophysical context to describe soft membranes [19], may be used as geometric model for graphene [20] capturing the sheet's bending energy. This model is given in terms of the energy functional $H[\mathbf{X}] = \int \mathrm{d}^2x\sqrt{g}\left[\frac{\alpha}{2}K^2 + \kappa_G R + \sigma\right]$, where $K = g^{ab}K_{ab}$ is the mean curvature, being g^{ab} the inverse metric tensor and g the metric determinant. R is the Ricci curvature, related to the extrinsic curvature by the Gauss-Codazzi equation, $R = K^2 - K_{ab}K^{ab}$ which by Gauss "egregium" theorem, depends solely on the metric tensor g_{ab}. The energy functional consists of three terms: the first term is the bending energy, being $\alpha > 0$ the bending rigidity; the second term is the Gaussian bending energy, being κ_G the Gaussian bending stiffness; and the third is a surface energy term, where $\sigma > 0$, called surface tension in the soft matter literature, is a Lagrange multiplier to fix the overall area of the membrane [19]. In this sense, α and κ_G are the only phenomenological parameters of our model. Furthermore, for a compact surface Σ, the second term $\int \mathrm{d}^2x\sqrt{g}R$ is a topological invariant known as the Euler characteristic $\chi(\Sigma)$.

Now, the Dirac fields confined to the surface may in principle, provoke modifications to the geometry of the membrane through thermal fluctuations on the fermion gas in the material. To determine an estimation of these effect in the geometry, we pose a correction to the elastic bending energy, $H_{\text{eff}}[\mathbf{X}] = H[\mathbf{X}] + \delta H_{\text{fermion}}[\mathbf{X}]$, where $\delta H_{\text{fermion}}[\mathbf{X}] = -\frac{g_v g_s}{\beta}\log Z(\beta, g)$ is the effective action from the Dirac field, being the factor g_v the valley and spin degeneracy g_s (in case of graphene), and β is the inverse of the thermal energy $k_B T$, where k_B is the Boltzmann constant and T is the temperature. Also, $Z(\beta, g)$ is the Dirac field partition function,

$$Z(\beta, g) = \int \mathscr{D}\Psi^\dagger \mathscr{D}\Psi e^{-\int_0^\beta \mathrm{d}\tau \int_\Sigma \mathrm{d}^2x\sqrt{g}\Psi^\dagger(\partial_\tau + \mathcal{H})\Psi}, \quad (1)$$

where $\mathcal{H} = -i\hbar v_F \gamma^0\underline{\gamma}^a\nabla_a$, with $\nabla_a = \partial_a + \Omega_a$, the spinorial covariant derivative and Ω_a is the spin-connection. Note that the operator $\partial_\tau + \mathcal{H}$ coincide with the Dirac operator in $2+1$ using the imaginary time x_0 by calling $\tau = -ix_0/(\hbar v_F)$, thus it is not difficult to show that $\partial_\tau + \mathcal{H} = -\hbar v_F\gamma^0\left[i\gamma^0\partial_0 + i\underline{\gamma}^a\nabla_a\right] = \hbar v_F\gamma^0\not{D}$, where the massless Dirac operator $\not{D} = -i\gamma^\mu\nabla_\mu$. Indices $\mu, \nu = 0, 1, 2$ are the local indices of the product manifold $S^1 \times \Sigma$.

Effective free energy for a 2D Dirac material. To calculate the functional integral (1), let us perform a usual decomposition in Fourier modes, details and conventions can be found in the Supplemental Material. Since the Dirac field is decomposed in Grassmann variables $\{\psi_n(x)\}$, it is known that Fermionic path integral can be carried out directly as

$$Z = \prod_{n\in\mathbb{Z}} \det{}_{\mathbb{H}}\left\{\left(i\omega_n\gamma^0 + \not{D}_E\right)\right\} \quad (2)$$

where ω_n are the fermionic Matsubara frequencies and $\not{D}_E = \gamma^0\hat{\mathcal{H}} = i\underline{\gamma}^a\nabla_a$ is an Euclidean Dirac operator, and $\mathbb{H}$ is the Hilbert space associated with spinorial functions on the curved surface Σ. Since we are using the signature $(-1, 1, 1)$ one has that $(\gamma^0)^\dagger = -\gamma^0$ and $(\gamma^a)^\dagger = \gamma^a$, thus the operator $i\omega_n\gamma^0 + \not{D}_E$ is self-adjoint. Now, using the identity $\log\det_{\mathbb{H}}\mathscr{O} = \mathrm{Tr}_{\mathbb{H}}\log\mathscr{O}$ and recalling that $\log\lambda = -\int_0^\infty \frac{\mathrm{d}s}{s}e^{-\lambda s}$ up to a divergent constant, (2) may be rewritten as,

$$\log Z = -\frac{1}{2}\int_0^\infty \frac{\mathrm{d}s}{s}\left(\sum_{n\in\mathbb{Z}} e^{-\omega_n^2 s}\right)\int_\Sigma \mathrm{d}A\ K(s, x, x), \quad (3)$$

where $dA = \mathrm{d}^2x\sqrt{g}$ is the surface area element and $K(s; x, x') = \langle x\left|e^{-Ds}\right|x'\rangle$ the Heat-Kernel of the operator $D = (\hbar v_F)^2\not{D}_E^2$ on Σ [21, 22]. To compute $\log Z$ let us focus on its integrand. The Heat-Kernel may be expanded in geometric invariants E_k as

$$K(s; x, x) = \frac{1}{4\pi}\sum_{k\geq 0}(s\hbar^2 v_F^2)^{k-1}\mathrm{tr}(E_k), \quad (4)$$

with tr being the pseudo-spin trace. The first coefficients E_k on a manifold without boundaries are local $O(2)$ invariant quantities [21]. In 2D, the Ricci scalar curvature R is the only independent component of the Riemann tensor $R_{abcd} = Rg_{a[c}g_{d]b}$, allowing us to evaluate E_k in

terms of R,

$$E_0 = \mathbb{1}, E_1 = -\frac{\mathbb{1}}{12}R, E_2 = -\frac{\mathbb{1}}{120}\left(\Delta_g R + \frac{1}{2}R^2\right). \quad (5)$$

Eq. (3) may be locally expanded according to (4), recasting the Matsubara sum in terms of the Jacobi theta function ϑ_4, $\log Z$ becomes

$$-\frac{1}{2}\int_0^\infty \frac{\mathrm{d}s}{s}\vartheta_4\left[\tfrac{i\ell_T^2}{4\pi s}\right]\sum_{k\geq 0}\frac{s^{k-\frac{3}{2}}}{(4\pi)^{3/2}\ell_T^{-1}}\int_\Sigma \mathrm{d}A\ \mathrm{tr}(E_k), \quad (6)$$

where $\ell_T = \hbar v_F/k_B T$ corresponds to the effective thermal wavelength. The zero temperature limit may be recovered from (6) noting that $\vartheta_4 \to 1$, consistent with the findings at [23]. Hence, from (6) defining the Heat-Kernel expansion coefficients at finite temperature as $a_k(x;\ell_T^2/s)$,

$$-\frac{1}{2}\int_0^\infty \frac{\mathrm{d}s}{s}\int_{S^1\times\Sigma}\frac{\mathrm{d}V}{(4\pi)^{3/2}}\sum_{k\geq 0}a_k(x;\ell_T^2/s)s^{k-\frac{3}{2}}$$

the coefficients are now be related to those at zero temperature as $a_k(x;\ell_T^2/s) = (\hbar v_F)\vartheta_4[i\ell_T^2/4\pi s]\mathrm{tr}(E_k)$ with the Jacobi function carrying the temperature dependence. The divergent part of the effective action is contained in $s \to 0$. At this limit, however, the expansion coefficients are exponentially suppressed, behaving as their zero temperature counterpart. Thus, finite temperature does not modify the divergent structure so the same counter-terms suffice for renormalization. To capture the IR divergence in (6) we introduce a UV cutoff Λ^{-2} and integrate up to some constant s_0 which may be taken to be arbitrary small. As argued above, at $s \to 0$ the coefficients are those at zero temperature allowing for the explicit integration of s. Disposing of the s_0 term, the divergent part reads,

$$-\frac{1}{\ell_T}\int_\Sigma \frac{\mathrm{d}A}{(4\pi)^{3/2}}\sum_{k=0}^{[3/2]}\mathrm{tr}(E_k)\frac{\Lambda^{3-2k}}{2k-3}, \quad (7)$$

leading to a counter-term effective Lagrangian density $c_1\Lambda^3 + c_2 R\Lambda$ with the constants $c_{1,2}$ determined from (7). Rescaling $s \to \ell_T^{-2}s$ the renormalized free energy becomes,

$$F_{\mathrm{ren}}[\mathbf{X}] = \frac{1}{2\beta}\sum_{k\geq 0} g_k^{\mathrm{ren}}\ell_T^{2k-2}\int_\Sigma \frac{\mathrm{d}A}{4\pi}\mathrm{tr}(E_k), \quad (8)$$

with g_k^{ren} constants determined by the Mellin transform of the Jacobi theta function,

$$g_k^{\mathrm{ren}} := \frac{1}{\sqrt{4\pi}}\int_0^\infty \mathrm{d}s\, s^{k-\frac{5}{2}}\left(\vartheta_4\left[\tfrac{i}{4\pi s}\right] - \nu_k\right) \quad (9)$$

where ν_k, defined as $\nu_{0,1} = 1$ and $\nu_{k\geq 2} = 0$, encapsulates the effect of renormalization procedure.

Thus the fermionic contribution to the free energy is $\delta H_{\mathrm{fermion}}[\mathbf{X}] = g_v g_s F_{\mathrm{ren}}[\mathbf{X}]$. The coefficients can be analytically obtained; $g_0^{\mathrm{ren}} = -3\zeta(3)$, $g_1^{\mathrm{ren}} = -2\log(2)$ and $g_2^{\mathrm{ren}} = 1/4$ for $k \geq 2$ in general, $g_k^{\mathrm{ren}} = 2\pi^{2-2k}[1 - 4^{1-k}]\Gamma(k-1)\zeta(2k-2)$ are monotonically decreasing. A strong curvature regime would require to include higher order contributions but these quickly suppressed by the increasing powers of ℓ_T limited by the validity of the Dirac model, for most relevant systems $k > 2$ contributions can be neglected.

Effective shape equation. The effective Hamiltonian obtained after integrating out the Dirac degrees of freedom and performing the renormalization procedure has the following structure

$$H_{\mathrm{eff}}[\mathbf{X}] = \int_\Sigma \mathrm{d}A\left[\frac{\alpha}{2}K^2 + \kappa_G^{\mathrm{eff}}R + \sigma_{\mathrm{eff}} + \frac{1}{2}\kappa_G^{(2)}R^2\right], \quad (10)$$

where $\sigma_{\mathrm{eff}} := \sigma + \delta\sigma_{\mathrm{eff}}$, $\kappa_G^{\mathrm{eff}} := \kappa_G + \delta\kappa_G^{\mathrm{eff}}$, i.e. with the exception of the bending rigidity coefficient α, all coefficients are modified by one-loop quantum corrections of the fermionic sector. The surface tension and Gaussian elastic module receive a temperature-dependent contribution stemming from the IR dynamics; $\beta\delta\sigma_{\mathrm{eff}} = -3g_v g_s\zeta(3)/\ell_T^2$ and $\beta\delta\kappa_G^{\mathrm{eff}} = \frac{1}{6}g_v g_s\log(2)$ respectively. It is noteworthy to notice the sign of $\delta\sigma_{\mathrm{eff}}$ associated with vacuum energy, this contribution will manifest in temperature constraints for the observation of carbon structures, discussed later. In addition, $\delta\sigma_{\mathrm{eff}}$ is in agreement with the known expression for the heat capacity of graphene in the Dirac approximation [6], as well as the Casimir-type contribution from the finite temperature calculation [24]. In contrast, an R^2 term has been induced with an emergent elastic coefficient $\beta\kappa_G^{(2)} = -\frac{g_v g_s}{960\pi}\ell_{\mathrm{T}}^2$. This term is already a consequence of the general expression obtained by the heat-kernel expansion in 2-dimensions [22], considered in [24] to determine if the sphere is a *global maximum* of their free energies.

Now, the natural question that arises is, what are the shapes that minimize the above effective Hamiltonian? To answer this question, we implement the auxiliary variable method introduced in [25] to obtain the shape equation of the membrane and its stress tensor described by the effective free energy (10). The basic idea is the introduction of Lagrange multipliers to impose the geometrical identities as holonomic constraints. In this procedure, an energy functional of the form $H[\mathbf{X}] = \int \mathrm{d}A\ \mathcal{H}[K_{ab}, g_{ab}, R]$ is replaced by a new functional that includes all geometrical necessary constraints (see Supplementary Material). Particularly, this extended functional includes $\int \mathrm{d}A\ \mathbf{f}^a \cdot (\mathbf{e}_a - \partial_a\mathbf{X})$, with the Lagrange multiplier $\mathbf{f}^a$ anchoring the tangent vector $\mathbf{e}_a$ to the embedding functions $\mathbf{X}$. Furthermore, $\mathbf{f}^a$ is the Nöether current associated to the translational invariance of the membrane $\mathbf{X} \to \mathbf{X} + \mathbf{a}$, for any $3D$ constant vector $\mathbf{a}$; consequently, $\mathbf{f}^a$ satisfies a conservation law $\nabla_a\mathbf{f}^a = 0$.

In addition, $\mathbf{f}^a$ is interpreted as the stress tensor of the membrane that, using the auxiliary method, can be expressed as $\mathbf{f}^a = \left(T^{ab} - \mathcal{H}^a{}_c K^{cb} + R\mathcal{H}_R g^{ab}\right)\mathbf{e}_b - \left[\nabla_b \mathcal{H}^{ab} - 2\left(\nabla_b \mathcal{H}_R\right)\left(g^{ab}K - K^{ab}\right)\right]\mathbf{N}$, where $T^{ab} = -2\frac{1}{\sqrt{g}}\partial(\sqrt{g}\mathcal{H})/\partial g_{ab}$ is the intrinsic stress tensor, $\mathcal{H}^{ab} := \partial\mathcal{H}/\partial K_{ab}$, $\mathcal{H}_R = \partial\mathcal{H}/\partial R$, and $\mathbf{N}$ is the unit normal vector to the surface. Decomposing $\mathbf{f}^a = f^{ab}\mathbf{e}_b + f^a\mathbf{N}$, the shape equation follows from the condition $\nabla_a f^a - K^{ab} f_{ab} = 0$ [25].

For the effective Hamiltonian (10) one has $\mathcal{H}_R = \kappa_{\rm eff}^G + \kappa_G^{(2)} R$, $\mathcal{H}^{ab} = \alpha g^{ab} K$, and the intrinsic stress tensor $T^{ab} = \frac{\alpha}{2}K\left(4K^{ab} - Kg^{ab}\right) - \left(\sigma_{\rm eff} + \kappa_G^{\rm eff} R + \frac{1}{2}\kappa_G^{(2)} R^2\right) g^{ab}$. Therefore the tangent, and normal components of the stress tensor are

$$f^{ab} = \alpha K\left(K^{ab} - \frac{1}{2}g^{ab}K\right) - g^{ab}\left(\sigma_{\rm eff} - \frac{\kappa_G^{(2)}}{2}R^2\right), \quad (11)$$

$$f^a = -\left[\alpha\nabla^a K + 2\kappa_G^{(2)}\nabla_b R\left(g^{ab}K - K^{ab}\right)\right], \quad (12)$$

respectively. Using the stress tensor, one can compute the force that a piece, $\mathscr{R}$, of the membrane acts on its surroundings. Indeed, according to the development in [19] this force is given by $\int_{\partial\mathscr{R}} ds\, \ell_a \mathbf{f}^a$, where ds is the line element on the boundary $\partial\mathscr{R}$, and ℓ_a are the components of the unit normal vector outward $\partial\mathscr{R}$. Furthermore, the shape equation turns out to be given by

$$-\alpha\left[\Delta_g K + \frac{1}{2}K\left(K^2 - 2R\right)\right] + \sigma_{\rm eff}K + 2\kappa_G^{(2)}\left[\left(K^{ab} - g^{ab}K\right)\nabla_a\nabla_b R - \frac{1}{4}R^2 K\right] = 0. \quad (13)$$

Notice that $\kappa_G^{\rm eff}$ does not appear in the shape equation, this is consequence of limiting our analysis to manifolds without boundaries, resulting in R-term of the effective Hamiltonian being topological. Despite the non-linear nature of the shape equation (13), it is possible to deduce exact solutions corresponding to known structures constructed from graphene.

On one hand, $R = 0$ and $K = 1/r_0$ constant are a solution of (13) which corresponds to a cylinder with radius $r_0 = \sqrt{\alpha/(2\sigma_{\rm eff})}$ while $\sigma_{\rm eff} > 0$. Likewise, taking the condition $K^2 = 2R$ and $K = 2/r_1$ constant, one get another solution of the equation (13) which corresponds to a sphere with radius $r_1 = (2\kappa_G^{(2)}/\sigma_{\rm eff})^{1/4}$ while $\sigma_{\rm eff} < 0$. The condition $\sigma_{\rm eff} > 0$ ($\sigma_{\rm eff} < 0$) for cylinder (sphere) imposes an upper (lower) bound on the equilibration temperature $T < T_{\rm c}$ ($T > T_{\rm c}$), where $T_{\rm c} = \left(\frac{\sigma(\hbar v_F)^2}{3g_v g_s \zeta(3) k_B^3}\right)^{\frac{1}{3}}$. In particular, for the cylinder surface, the mean curvature and Ricci curvature satisfy

$$K_{\rm cyl} = \frac{1}{\ell_{T_{\rm c}}}\sqrt{\frac{6g_v g_s \zeta(3) k_B T_{\rm c}}{\alpha}}\left[1 - \left(\frac{T}{T_{\rm c}}\right)^3\right]^{\frac{1}{2}}, \qquad R_{\rm cyl} = 0 \quad (14)$$

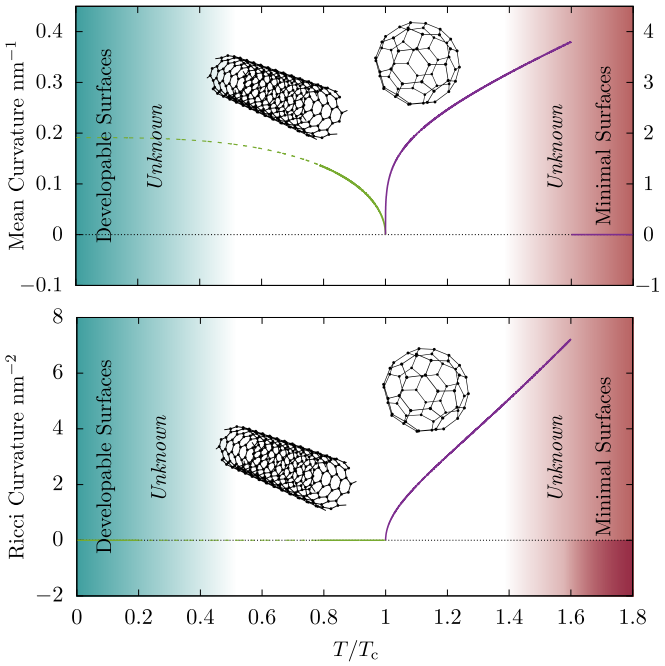

FIG. 1. Mean and Ricci curvature as a functions of temperature. The green (purple) lines denote the values for cylindrical (spherical) structures in the nm scale. The solid lines shows the stability region starting at $T_{\rm min} = 757.75\,$K for carbon nanotubes. The critical temperature $T_{\rm c} = 963.16\,$K is obtained imposing the constraints $r_{C60} < 1\,$nm and $r_{\rm nt} < 8\,$nm at synthesis temperatures $T_{C60} = 1000\,$K and $T_{\rm nt} = 720\,$K within range of the known values in the literature [26]. The values of $T_{\rm min}$ and T_c has been obtain using $\alpha = 1.44$ eV [20], and Fermi velocity $v_F = 0.85 \times 10^6\,$m/s [27].

whereas for the sphere surface, these curvatures satisfy

$$K_{\rm sph} = \frac{2(1440\pi\zeta(3))^{\frac{1}{4}}}{\ell_{T_{\rm c}}}\left(\frac{T}{T_{\rm c}}\right)^{\frac{1}{4}}\left[\left(\frac{T}{T_{\rm c}}\right)^3 - 1\right]^{\frac{1}{4}}, \qquad R_{\rm sph} = \frac{1}{2}K_{\rm sph}^2 \quad (15)$$

Clearly, the temperature $T_{\rm c}$ distinguishes two separated phases where cylindrical and spherical surface formation occurs. This distinction is a consequence of the contrast dependence of the effective elastic coefficients with respect to the thermal wavelength; indeed, while surface tension coefficient behaves as $\beta\delta\sigma_{\rm eff} \sim \ell_T^{-2}$, the non-linear elastic coefficient as $\beta\kappa_G^{(2)} \sim \ell_T^2$. This is another way to see that there are two opposite temperature regimes for the formation of the surfaces. By convenience, we call the high- and low-temperature regimes, these dominions can be defined by $T \gg T_{\rm c}$ and $T \ll T_{\rm c}$, respectively, where $T_{\rm c}$ is the same characteristic temperature defined above. Notice that in the low-temperature regime, the density energy $\frac{1}{2}\beta\kappa_G^{(2)}R^2$ dominates the elastic behavior, while in the high-temperature region, the term $\delta\sigma_{\rm eff}$ dominates the behavior. In the low-temperature regime, the shape equation reduces to $\left(K^{ab} - g^{ab}K\right)\nabla_a\nabla_b R - \frac{1}{4}R^2 K = 0$.

Notice that this equation is identically satisfied for $R = 0$. Thus, all surfaces with $R = 0$ represent solutions in this regime, encompassing various types of geometric configurations known as *developable surfaces*; generated by sweeping a straight line in space and revolving around an axis: planes, cylinders, conical surfaces, tangent surfaces, and union of pieces of them [28]. In addition, in the high-temperature dominion, the shape equation reduces to $\delta\sigma_{\text{eff}}K = 0$ or $K = 0$, which corresponds to a plethora of structures known as *minimal surfaces* [28].

A phase diagram for the conformation of surfaces above is depicted in Fig. 1 through the mean and Ricci curvatures versus the reduced temperature T/T_c. The phase diagram shows six regions, from left to right, a developable surface phase for $T \ll T_c$, a cylinder phase for $T < T_c$, a sphere phase for $T_c < T$, a minimal surface phase for $T \gg T_c$ and two unknown regions. Notice that from the solutions (14) and (15) we cannot either infer a lower value of temperature for cylinder neither a upper value of temperature for sphere phase. However, we can deduce these temperature values if we perform a mechanical stability analysis (see Supplemental Material for details). Indeed, through the calculation of the second variation of the effective Hamiltonian (10), the condition for the cylinder to be stable is the inequality $T > c_{\text{cyl}}T_c(1-(T/T_c)^3)$, whereas for the sphere $T > c_{S^2}T_c((T/T_c)^3 - 1)$, with c_{cyl} and c_{S^2} at the Supplemental Material. The large value of $T_{\max}$ obtained for the sphere, implies their stability to all practical values of temperature. In addition, the minimal surfaces solutions under the Hamiltonian $\int \delta\sigma_{\text{eff}}dA$ are unstable, however, if we do not neglect the bending energy $\frac{\alpha}{2}\int dAK^2$ the shape equation reduce to $-\alpha\left[\Delta_g K + \frac{1}{2}K\left(K^2 - 2R\right)\right] + \sigma_{\text{eff}}K = 0$, where still $K = 0$ is a solution but now the surfaces are stable. Therefore the stable minimal surfaces are found in the high-temperature regime neglecting the terms $\kappa_G^{(2)}$ but not the bending coefficient α. In contrast, the developable surface of graphene dominated by the term $\frac{1}{2}\kappa_G^{(2)}R^2$ appears to be unstable under mechanical deformation.This instability may be related to the tendency of the membrane to crumple [14].

Concluding remarks. We have provided for the first time a simple theoretical phase diagram of the shapes that a curved sheet of graphene can have under the assumption that the electronic degrees of freedom are described by the Dirac curved model. From this perspective, more realistic modeling of curved graphene would require including a non-abelian Wilson line to account for topological defects that result in non-trivial curvature. It would be interesting to see how such corrections translate to shape equations, stability, and consequently to the phase diagram, to be reported elsewhere. Additionally, a curved tight-binding model that provided the correct field theory at low energy would aim to understand the possible carbon shapes accurately; a discussion in this direction is provided in [8–10]. However, it is noteworthy that despite the simple and naïve model for curved graphene used here, captures most of the equilibrium geometries obtained with the shape equation (13) have been experimentally observed for graphene. Cylinder and spherical surfaces correspond to the well-known single-wall carbon nanotube and Buckminsterfullerene C_{60} structures with observed characteristic radii around $\sim$1 nm. Furthermore, according to the thermal pyrolysis synthesis method for the formation of carbon nanotubes (CNTs), presented in [12], the CNT formation rate increases above 700 K and decreases after 1000 K, which is in agreement, qualitatively, with the cylindrical phase of the phase diagram shown in Fig. (1). According to [26], fullerenes C_{60} and C_{70} are not formed at 298.15 K, but they can be produced at 1273.15 K. These findings are consistent with the spherical phase shown in Fig. (1). Although negative Gaussian curvature has not been produced in the lab or found in nature, there is a reasonable expectation to do so; in particular, it may be necessary to seek the synthesis of membranes with negative curvature surfaces at higher temperatures according to the above phase diagram, despite the current experimental obstacles. However, minimal surfaces are currently considered candidates to understand Glass-like Carbon [2]. In this way, the negative Casimir-like contribution from fermions imposes a tight constraint on the classical contribution to the surface tension σ, or equivalently, the critical temperature T_c to be measured at the lab.

As a matter of perspectives, it would be interesting to explore what other *types* of solutions, i.e. expected surfaces, Eq. (13) allows. However, as evidenced via Monge gauge, the shape equation often results in a complicated nonlinear fourth-order differential equation for the height function where appropriate boundary conditions and approximations should be carefully considered. In the case of graphene, consistency (13) with the currently observed structures predicts a strict bound on the values for the surface tension of the fermionic membrane. However, under a conformal transformation, the shape equation (13) constrains the conformal factor, resulting in a more tractable second-order PDE to explore nontrivial deformations of simple geometries. Additionally, including an electromagnetic field would provide extrinsic curvature terms that, under the integration of the fermionic degrees of freedom, may correct the bending parameter since the electromagnetic fields are in the ambient space where the membrane is embedded.

* pablo_morales@araya.org
† pcastrov@unach.mx; author to whom correspondence should be addressed.

[1] A. H. Castro Neto, F. Guinea, N. M. R. Peres, K. S. Novoselov, and A. K. Geim, Rev. Mod. Phys. **81**, 109 (2009).

[2] P. Mélinon, Nanomaterials **11**, 10.3390/nano11071694 (2021).
[3] K. S. Novoselov, A. K. Geim, S. V. Morozov, D. Jiang, M. I. Katsnelson, I. V. Grigorieva, S. V. Dubonos, and A. A. Firsov, Nature **438**, 197 (2005).
[4] G. G. Naumis, S. Barraza-Lopez, M. Oliva-Leyva, and H. Terrones, Reports on Progress in Physics **80**, 096501 (2017).
[5] N. Levy, S. A. Burke, K. L. Meaker, M. Panlasigui, A. Zettl, F. Guinea, A. H. C. Neto, and M. F. Crommie, Science **329**, 544 (2010), https://www.science.org/doi/pdf/10.1126/science.1191700.
[6] P. Castro-Villarreal and R. Ruiz-Sánchez, Phys. Rev. B **95**, 125432 (2017).
[7] P. A. Morales and P. Copinger, Phys. Rev. B **107**, 075432 (2023).
[8] M. M. Roberts and T. Wiseman, Phys. Rev. B **105**, 195412 (2022); Phys. Rev. B **109**, 045425 (2024).
[9] A. Iorio and P. Pais, Phys. Rev. B **106**, 157401 (2022).
[10] M. M. Roberts and T. Wiseman, Phys. Rev. B **106**, 157402 (2022).
[11] A. d. J. Espinosa-Champo, G. G. Naumis, and P. Castro-Villarreal, arXiv preprint arXiv:2310.07920 (2023).
[12] P. Srisuma, N. Suwattanapongtada, N. Opasanon, P. Charoensuppanimit, K. Kerdnawee, C. Termvidchakorn, W. Tanthapanichakoon, and T. Charinpanitku, Engineering Science and Technology, an International Journal **24**, 1373 (2021).
[13] A. Chuvilin, U. Kaiser, E. Bichoutskaia, N. A. Besley, and A. N. Khlobystov, Nature Chemistry **2**, 450 (2010).
[14] S. Fischetti, L. Wallis, and T. Wiseman, Phys. Rev. Lett. **120**, 261601 (2018).
[15] D. Kolesnikov and V. Osipov, The European Physical Journal B-Condensed Matter and Complex Systems **49**, 465 (2006).
[16] S. Iijima, Nature **354**, 56 (1991).
[17] H. Terrones and A. Mackay, Carbon **30**, 1251 (1992).
[18] P. Canham, Journal of Theoretical Biology **26**, 61 (1970); W. Helfrich, Z Naturforsch C **28**, 693 (1973).
[19] M. Deserno, Chemistry and Physics of Lipids **185**, 11 (2015), membrane mechanochemistry: From the molecular to the cellular scale.
[20] Y. Wei, B. Wang, J. Wu, R. Yang, and M. L. Dunn, Nano Letters **13**, 26 (2013), pMID: 23214980, https://doi.org/10.1021/nl303168w.
[21] L. Parker and D. Toms, *Quantum Field Theory in Curved Spacetime: Quantized Fields and Gravity*, Cambridge Monographs on Mathematical Physics (Cambridge University Press, 2009).
[22] D. Vassilevich, Physics Reports **388**, 279 (2003).
[23] H. Boschi-Filho and C. P. Natividade, Phys. Rev. D **46**, 5458 (1992).
[24] S. Fischetti, L. Wallis, and T. Wiseman, Journal of High Energy Physics **2020**, 1 (2020).
[25] J. Guven, Journal of Physics A: Mathematical and General **37**, L313 (2004).
[26] T. Sugai, H. Omote, S. Bandow, N. Tanaka, and H. Shinohara, The Journal of Chemical Physics **112**, 6000 (2000), https://pubs.aip.org/aip/jcp/article-pdf/112/13/6000/19295065/6000_1_online.pdf.
[27] C. Hwang, D. A. Siegel, S.-K. Mo, W. Regan, A. Ismach, Y. Zhang, A. Zettl, and A. Lanzara, Scientific reports **2**, 590 (2012).
[28] M. P. do Carmo, *Differential geometry of curves and surfaces*. (Prentice Hall, 1976) pp. I–VIII, 1–503.
[29] R. Capovilla, J. Guven, and J. Santiago, Journal of Physics A: Mathematical and General **36**, 6281 (2003).

SUPPLEMENTAL MATERIAL

Notation and Fourier decomposition of the Dirac Field

Let us perform a decomposition in Fourier modes as follows

$$\Psi(\tau,x) = \frac{1}{\sqrt{\beta}}\sum_{n\in\mathbb{Z}}\psi_n(x)\,e^{-i\omega_n\tau}, \tag{16}$$

$$\psi_n(x) = \frac{1}{\sqrt{\beta}}\int_0^\beta d\tau\Psi(\tau,x)e^{i\omega_n\tau} \tag{17}$$

where $\omega_n=(2n+1)\pi/\beta$, with $n\in\mathbb{Z}$, are the Matsubara frequencies. Orthogonality relations for the Fourier basis is $\int_0^\beta d\tau e^{i\tau(\omega_n-\omega_{n'})}=\beta\delta_{nn'}$, and completeness relationship $\sum_{n\in\mathbb{Z}}e^{i\omega_n(\tau-\tau')}=\beta\delta(\tau-\tau')$. Using the Fourier decomposition of the Dirac field, and the orthogonality relation, the action adopts the following frequency representation

$$S(\Psi^\dagger,\Psi)=\sum_{n\in\mathbb{Z}}\int_\Sigma d^2x\sqrt{g}\;\psi_n^\dagger(x)\left(-i\omega_n+\hat{\mathscr{H}}\right)\psi_n(x)$$

The functional measure in the Fourier basis is written as $\mathscr{D}\left(\Psi^\dagger,\Psi\right)=\prod_{n\in\mathbb{Z}}\mathscr{D}\left(\psi_n^\dagger,\psi_n\right)$, thus the functional integral adopts the following expression

$$Z=\prod_{n\in\mathbb{Z}}\left[\int\mathscr{D}\left(\overline{\psi}_n,\psi_n\right)e^{-\int_\Sigma d^2x\sqrt{g}\;\overline{\psi}_n(x)\left(i\omega_n\gamma^0+\not{D}_E\right)\psi_n(x)}\right]$$

where $\not{D}_E=\gamma^0\hat{\mathscr{H}}=i\underline{\gamma}^a\nabla_a$ is an Euclidean Dirac operator. Since $\{\psi_n(x)\}$ are Grassmann variables, it is known that each of these integrals can be carried out directly, thus we get the Eq. (2) from the manuscript.

Heat-Kernel expansion

Let us here make a few comments on the local expansion of the Heat-Kernel (4). As described [22] the asymptotic behaviour of $K(s;x,x)$ goes as $s^{(k-m)/2}$ with 2 corresponding to the degree of the operator, m the dimension of the manifold and $k\in\mathbb{Z}^+$ to the k-th leading term. For manifolds without imposed boundaries, it can be shown that only k even contribute, relabeling coincides with the standard notation at [21] adopted in this paper. The coefficients read,

$$E_0=\mathbb{1}\,,\quad E_1=-\frac{\mathbb{1}}{12}R\,, \tag{18}$$

$$E_2 = \frac{1}{12}\Lambda^{\mu\nu}\Lambda_{\mu\nu} + \frac{\mathbb{1}}{180}[R^{\mu\nu\rho\sigma}R_{\mu\nu\rho\sigma} - R^{\mu\nu}R_{\mu\nu}] - \frac{1}{6}\nabla_\mu\nabla^\mu\left(\tfrac{1}{5}R - X\right)\mathbb{1} + \frac{1}{2}(\tfrac{1}{6}R - X)^2\mathbb{1}\,, \quad (19)$$

with $\Lambda_{\mu\nu} = [\nabla_\mu, \nabla_\nu] = -iR^{ab}{}_{\mu\nu}\Sigma_{ab}$, where $\Sigma_{ab} = -\frac{i}{8}[\gamma_a, \gamma_b]$ corresponds to the generators of the Lorentz group, $X = \frac{1}{4}R$ for the elliptic Dirac operator.

Stress tensor and shape equation

First variation of the effective Hamiltonian by auxiliary variables

Following [25], here we introduce the auxiliary variables method. To thus purpose, we introduce the functional $H_c\left[\mathbf{X}, R, K_{ab}, g_{ab}, \mathbf{e}_a, \mathbf{N}, \Lambda^{ab}, \mathbf{f}^a, \lambda_n, \lambda_{ab}, \lambda^a_\perp\right] := H_c$ where H_c is given by

$$\begin{aligned} H_c &= \int \mathrm{d}A\ \mathcal{H}\left[K_{ab}, g_{ab}, R\right] + \int \mathrm{d}A\ \mathbf{f}^a \cdot (\mathbf{e}_a - \partial_a\mathbf{X}) \\ &+ \int \mathrm{d}A\left(\lambda^a_\perp\left(\mathbf{e}_a\cdot\mathbf{N}\right) + \lambda_n\left(\mathbf{N}^2 - 1\right)\right) \\ &+ \int \mathrm{d}A\left(\Lambda^{ab}\left(K_{ab} - \mathbf{e}_a\cdot\partial_a\mathbf{N}\right) + \lambda^{ab}\left(g_{ab} - \mathbf{e}_a\cdot\mathbf{e}_b\right)\right) \\ &+ \int \mathrm{d}A\ \Lambda_R\left(R - (g^{ab}K_{ab})^2 + K_{ab}K_{cd}g^{ac}g^{db}\right) \quad (20) \end{aligned}$$

Now, we carry out variations respect to each quantity. Let us performed the variation respect to K_{ab}. Thus it is convenient to define $\mathcal{H}^{ab} := \frac{\partial\mathcal{H}}{\partial K_{ab}}$ and $\mathcal{H}_R = \frac{\partial\mathcal{H}}{\partial R}$. Thus we got the equation $\Lambda^{ab} = -\mathcal{H}^{ab} - 2\mathcal{H}_R(g^{ab}K - K^{ab})$. Now, we perform the variation with respect to the metric g_{ab}. Now, it is convenient to define $T^{ab} = -2\frac{1}{\sqrt{g}}\frac{\partial(\sqrt{g}\mathcal{H})}{\partial g_{ab}}$. This quantity is the intrinsic stress tensor, thus it is not difficult to show $\lambda^{ab} = \frac{T^{ab}}{2} + 2\mathcal{H}_R R^{ab}$, where we have used the definition of the Ricci curvature $R_{ab} = K_{ab}K - K_{ac}K^c{}_b$. Now, the variation with respect to the embedding functions $\mathbf{X}$. This variation represents a conservation principle $\nabla_a\mathbf{f}^a = 0$, where ∇_a is the covariant derivative compatible with the metric g_{ab}. Now, we carry out the variation with respect to $\mathbf{e}_a$. This equation gives us the stress tensor of the graphene membrane

$$\mathbf{f}^a = \left(\Lambda^{ac}K^b_c + 2\lambda^{ab}\right)\mathbf{e}_b - \lambda^a_\perp\mathbf{N}. \quad (21)$$

Now, we make the variation with respect to $\mathbf{N}$.

$$\lambda^a_\perp\mathbf{e}_a + 2\lambda_n\mathbf{N} + \nabla_a(\Lambda^{ab}\mathbf{e}_a) = 0 \quad (22)$$

Now, we use the Weingarten-Gauss equations, $\nabla_a\mathbf{e}_b = -\mathbf{K}_{ab}\mathbf{N}$, which implies

$$\begin{aligned} \lambda^a_\perp &= -\nabla_b\Lambda^{ab} \\ 2\lambda_n &= \Lambda^{ab}K_{ab} \end{aligned} \quad (23)$$

leading to the tangent and normal components at Eqns. (11) and (12).

Stability analysis of the geometric configurations

Second variation of the effective Hamiltonian

As shown in [29], the second variation of a surface functional invariant under parametrization $H[\mathbf{X}] = \int d^2x\sqrt{g}f(X)$ can always be expresed in the form

$$\delta^2 H = \int dA\Phi\mathscr{L}_f\Phi \quad (24)$$

for some local differential operator $\mathscr{L}$, where change in the embedding function is given by $\mathbf{X} \to \mathbf{X} + \delta\mathbf{X}$ with $\delta\mathbf{X} = \Phi\mathbf{n} + \Phi^a\mathbf{e}_a$. In addition, it has been assumed that the surfaces are closed without boundaries. In particular, the operator $\mathscr{L}$ can be obtained by performing the normal variation $\mathscr{L}\Phi = \delta_\perp(\sqrt{g}\mathscr{E}(f))$, where $\mathscr{E}(f)$ is the factor obtained in the first normal variation of the functional. In particular, the Euler-Lagrange equations are at equilibrium $\mathscr{E}(f) = 0$. Here, we focus on the second order variation of the functional $\frac{1}{2}\kappa_G^{(2)}\int dA\,R^2$ as the variation of the other terms in the effective Hamiltonian are already computed in [29]. After a tedious but straightforward calculation

$$\begin{aligned} \frac{1}{4}\mathscr{L}_{R^2} &= K\left[K^{ab}(\nabla_a\nabla_b R) - K(\Delta_g R) - \frac{1}{4}R^2K\right] + (\nabla_a\nabla_b R)\left[-\nabla^a\nabla^b + (KK^{ab} - R^{ab}) - 4K^{ac}K_c{}^b\right] \\ &+ (K^{ab} - Kg^{ab})\nabla_a\nabla_b\left[2\nabla_c\left[(K^{cd} - g^{cd}K)\nabla_d(\cdot)\right] - RK(\cdot)\right] - \nabla_c R\left[K^c_a\nabla_b + K^c_b\nabla_a - K_{ab}\nabla^c + (\nabla_a K^c_b)\right] \\ &- (\Delta_g R)\left[-\Delta_g + (R - K^2)\right] + 2KK^{ab}\nabla_a\nabla_b R + K\nabla_a K\nabla^a R + 2KK^{ab}\nabla_a R\nabla_b - K^2\nabla^a R\nabla_a \\ &- \frac{1}{2}RK\left[2\nabla_c\left[(K^{cd} - g^{cd}K)\nabla_d(\cdot)\right]\right] - \frac{1}{4}R^2\left(-\Delta_g + (R - K^2)\right). \end{aligned} \quad (25)$$

As in [29], one has the following expressions for the operators $\mathscr{L}_{K^2}$ and $\mathscr{L}_{K^2}$, defined in (24),

$$\begin{aligned} \mathscr{L}_{K^2} &= 2\Delta_g^2 + (K^2 - 4R)\Delta_g + 4KK^{ab}\nabla_a\nabla_a \\ &+ 2R^2 + 2K^4 - 5RK^2 + 12K^{ab}\nabla_a\nabla_b K \\ &- K\Delta_g K + (\nabla^a K)(\nabla_a K) \end{aligned} \quad (26)$$

and

$$\mathscr{L}_1 = -\Delta_g + R\,. \tag{27}$$

Stability analysis of the cylinder

In the case of the cylinder with parametrization $\mathbf{X}(\theta, z) = (r_0\cos\theta, r_0\sin\theta, z)$, where recall that the cylinder radius is $r_0 = \sqrt{\alpha/2\sigma_{\text{eff}}}$ is the radius of the cylinder, with $\sigma_{\text{eff}} > 0$. using this parametrization one have the surface metric components $g_{\theta\theta} = r^2$, $g_{zz} = 1$, $g_{\theta z} = g_{z\theta} = 0$, the components of the extrinsic curvature tensor $K_{\theta\theta} = r_0$, $K_{zz} = K^{zz} = K_{\theta z} = K^{\theta z} = K_{z\theta} = K^{z\theta} = 0$, and $K^{\theta\theta} = 1/r_0^3$. Additionally, the mean curvature $K = 1/r$ and the Ricci curvature $R = 0$. The Laplace-Beltrami operator on scalars is $\Delta_{\text{cyl}} = r_0^{-2}\partial_\theta^2 + \partial_z^2$. The spectrum of this operator is $-\frac{1}{r_0^2}(m^2 + (kr_0)^2)$, for $m \in \mathbb{Z}$ and $k \in \mathbb{R}$. Using $\mathscr{L}_{K^2}, \mathscr{L}_1$ and $\mathscr{L}_{R^2}$ we can compute the spectrum of the operator $\mathscr{L}_{\text{cyl}}$ for the energy density of the effective Hamiltonian,

$$\begin{aligned}\text{spec}(\mathscr{L}_{\text{cyl}}) = \frac{2\sigma_{\text{eff}}}{r_0^2}\left[m^4 + 2m^2((kr_0)^2 - 1) + 1\right] \\ + \frac{(2\sigma_{\text{eff}})^2}{\alpha}\left[1 + \frac{8\kappa_G^{(2)}\sigma_{\text{eff}}}{\alpha^2}\right](kr_0)^4\,.\end{aligned} \tag{28}$$

Observe that the first term is always positive, whereas the second term is only positive if the condition $1 + \frac{8\kappa_G^{(2)}\sigma_{\text{eff}}}{\alpha^2} > 0$. This implies the following inequality for the temperature

$$\frac{T_*}{1 - T_*^3} > c \tag{29}$$

where we have defined the reduce temperature $T_* = T/T_c$ and $c = \frac{8g_v g_s \ell_{T_c}^2 \sigma k_B T_c}{\alpha^2}$. The minimum value of the temperature where the cylinder configuration is stable is given by

$$\frac{T_{\min}}{T_c} = \left(\frac{2\lambda}{3}\right)^{\frac{1}{3}}\left[\frac{1}{2c}\left(\frac{2}{3}\right)^{\frac{1}{3}} - \lambda^{-\frac{2}{3}}\right] \tag{30}$$

with $\lambda = 9c^3 + \sqrt{3c^3(27c^3 + 4)}$ Additionally, one can show that the image of the RHS function of c is the interval $[0, 1]$ for any value of $c \in \mathbb{R}$.

Stability analysis of the sphere

In the case of the sphere, including an explicit parametrization is unnecessary. It is enough to use the fact that the curvature extrinsic tensor satisfies $K_{ab} = \frac{K}{2}g_{ab}$, and $K^2 = 2R$. We recall that the radius sphere satisfy $r_1 = (2\kappa_G^{(2)}/\sigma_{\text{eff}})^{1/4}$ or equivalently the Ricci curvature is $R = (2\sigma_{\text{eff}}/\kappa_G^{(2)})^{1/2}$, with $\sigma_{\text{eff}} < 0$. Also, we take the advantage that the Laplace-Beltrami operator on scalars for the sphere is written in terms of the angular momentum $\hat{\mathbf{L}}$ as $\Delta_{S^2} = -\frac{R}{2}\hat{\mathbf{L}}^2$, whose eigenvalues are given by $\ell(\ell+1)$, for $\ell \in \mathbb{N}\cup\{0\}$. The spectrum of the operator $\mathscr{L}_{\text{cyl}}$ for the energy density of the effective Hamiltonian is obtained using $\mathscr{L}_{K^2}, \mathscr{L}_1$ and $\mathscr{L}_{R^2}$ is

$$\text{spec}(\mathscr{L}_{S^2}) \;=\; \frac{1}{4}\alpha R^2 f_\ell^{(1)} + \frac{1}{2}\sigma_{\text{eff}} R f_\ell^{(2)} \tag{31}$$

where $f_\ell^{(1)} = \ell(\ell+1)\left[\ell(\ell+1) - 2\right]$ and $f_\ell^{(2)} = \left[2\left(\ell(\ell+1) - 2\right)\left(\ell(\ell+1) - \frac{5}{2}\right) + \ell(\ell+1) + 1\right]$. Notice that the sequence $f_\ell^{(1)} \geq 0$, whereas the sequences $f_\ell^{(2)} > 0$ for all $\ell \in \mathbb{N}\cup\{0\}$. The stability condition should satisfy $\text{spec}(\mathscr{L}_{S^2}) > 0$ for all ℓ, implying $(-2\sigma_{\text{eff}}/(\alpha R)) < f_\ell^{(1)}/f_\ell^{(2)}$. Now, notice that the new sequence $f_\ell^{(1)}/f_\ell^{(2)} \leq 24/35$. Substituting the expression of the Ricci curvature in terms of the temperature and a straightforward calculation, we obtain the condition

$$\frac{T_*^3 - 1}{T_*} < \left(\frac{24}{35}\right)^2 \frac{\alpha^2 1440\pi\zeta(3)}{\sigma^2 \ell_{T_c}^4} := d\,. \tag{32}$$

Recall that $T_* \geq 1$ since is the condition found in the sphere solution. Thus, the maximum value of T_* that satisfies the above inequality is the real root of the third-order polynomial $P(x) = x^3 - dx - 1$ for $x \geq 1$.

Stability analysis of the minimal surfaces

In the case of minimal surfaces $K = 0$, we use the operators $\mathscr{L}_{K^2}$, and $\mathscr{L}_1$. It is not difficult to show by integrating by parts that

$$\mathscr{L}_{\text{MinS}} = \alpha(-\Delta_g + R)^2 + \sigma_{\text{eff}}(-\Delta_g + R) \tag{33}$$

which certainly will give a positive spectrum. Note that $\alpha \neq 0$ or is required for stability. As a consequence, at high temperatures the contribution from σ_{eff} dominates resulting in $\text{spec}(\mathscr{L}_{\text{MinS}}) < 0$, i.e. unstable structures.

Stability analysis of the developable surfaces

In the case of developable surfaces $R = 0$, we use the operator $\mathscr{L}_{R^2}$. It is not difficult to show using the Codazzi-Mainardi equation $\nabla_a K^{ab} = \nabla^b K$ that

$$\mathscr{L}_{\text{DevS}} = 4\kappa_G^{(2)}\mathscr{O}^2 \tag{34}$$

where $\mathscr{O} = (K^{ab} - Kg^{ab})\nabla_a\nabla_b$. Since $\kappa_G^{(2)}$ is negative, the developable surfaces are automatically unstable.